LIFE DETECTION LIMITATIONS DUE TO FLUORESCENCE IN RAMAN IMAGING

Julienne Ruth Emry, Alison Olcott Marshall, and Craig Marshall

Introduction

Multiple studies have revealed that abiotic features, such as fluid inclusions or veins, may be misidentified as microfossils or other biosignatures [1-4]. In an attempt to avoid this problem, researchers have proposed a variety of criteria based on morphology, context, and chemistry that should all be met if a sample is to be considered a *bona fide* microfossil [2,5,6]. This has led to increased interest in the chemical composition of putative microfossils, and Raman spectroscopy has become a popular technique to study the composition of microfossils [2,3] and to detect other traces of life (see [7] and references therein). Additionally, the 2018 Exomars rover includes a Raman spectrometer [8] and the 2020 NASA rover will contain two Raman instruments, SuperCam and SHERLOC [9].

Recent technological advances have allowed for advanced Raman data collection including hyperspectral imaging, which has been used to study a variety of microfossils and microfossil-like features. [10-16], and to search for biomarkers [17]. Hyperspectral datasets are composed of multiple spectra aquired based on an operator-defined spatial resolution represented by the numbered circles on the schematic diagram of a Raman imaging experiment. The dashed boxes respresent a two-dimensional region of interest over which spectra can be collected at multiple focal depths (a) [18].The numbered circles (a) correspond to individual spectra acquired during data collection (b). In addition to natural processes, instrumental collecion parameters and analysis issues may mimic evidence for life in resulting Raman images. Many factors can affect spectral quality during data collection, but autofluorescence can be a problematic issue that limits the ability to acquire useful data [18]. Depending on the analytical method used, sloping base-lines caused by autofluorescence can result in Raman images that mistakenly indicate the presence carbon in regions where it is not, in fact, present.

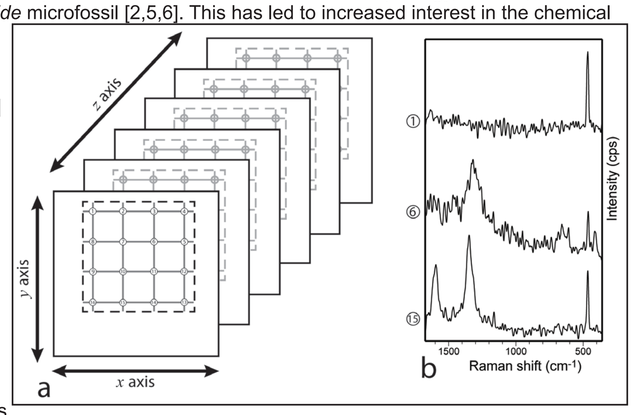

The Apex chart

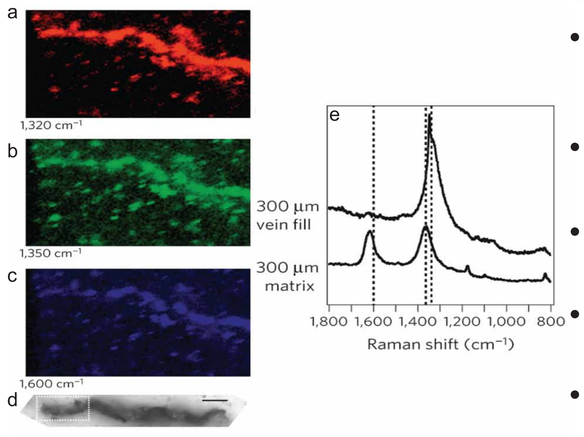

- **~3.5 Ga chert unit from the Pilbara craton, Western Australia contains microstructures described as among the earliest microbial fossils on earth**
- **Microstructures originally interpreted as carbonaceous based on point Raman spectroscopy and Raman imaging**
- **These structures were recently reinterpreted as hematite-filled microveins utlilizing Raman imaging**
- **Misinterpretation may have resulted from close proximity of the 1320 cm^{-1} hematite and the 1350 cm^{-1} carbon "D" band**
- **Intensity at 1600 cm^{-1} (carbon "G" band) should be used to identify carbon in Raman hyperspectral images**

Raman intensity at a point images representing hematite (a) and carbon (b,c) from a hyperspectral dataset acquired from an Apex chert microvein (d). Note the colocation of the 1320 cm^{-1} hematite band and the 1350 cm^{-1} carbon D band potentially resulting in misidentification of carbon in Raman images when using intensity at 1350 cm^{-1} (carbon "D") band to analyze Raman imaging datasets. Adapted from [3].

Astrobiological Implications

- **Autoflourescence may lead to false-positive identification of carbon and potentially ancient life**
- **Multivariate techniques can be used to identify carbon**
- **Multiple analytical techniques can provide robust interpretations**

Raman Spectroscopic Analyses

Raman spectroscopic analyses were conducted using a Renishaw Reflex Raman microprobe with an attached trinocular Leica DMLM microscope equipped with a video camera utilizing a 1000/0.9 NA objective lens. An argon-ion laser (Modu-Laser) emitting at 514.5 nm was used to excite the samples. A 2400/mm grating was used and spectra were analyzed at room temperature with a Peltier cooled, charge coupled device (CCD)(camera (1024x256 pixels). The system was calibrated by analyzing the position of the F_{1g} silicon mode. An offset correction was performed based on the position of the detected silicon band at 520.5 ± 0.1 cm^{-1}. Raman imaging datasets were collected using Renishaw Streamline^{TM} mode with an accumulation time of 0.1 sec. In Streamline^{TM} mode a center value is identified that defines the spectral range based on the instrumental parameters, in this case providing a range of ~1330 cm^{-1} from 360-1690 cm^{-1}. This range was selected so as to maximize inclsion of as many intense diagnostic Raman bands for all the materials present as possible. Two-dimensional datasets were collected at 0.2 micron intervals in depth over the same *x,y* region. The automatic cosmic ray removal feature provided by the Renishaw software was implemented. All images displayed were created by assigning the central 90% of the data to the software-based color interpolation algorythm.

ACKNOWLEDGEMENTS

This work was funded by NSF grant EAR-1053241

REFERENCES

[1]Bridgwater, D., J. H. Allaart, J. W. Schopf, C. Klein, M. R. Walter, E. S. Barghoorn, P. Strother, A. H. Knoll and B. E. Gorman (1981). "Microfossil-like objects from the Archaean of Greenland: a cautionary note." Nature 289(5793): 51-53. [2]Schopf, J. W., A. B. Kudryavtsev, K. Sugitani and M. R. Walter (2010). "Precambrian microbe-like pseudofossils: A promising solution to the problem." Precambrian Research 179(1–4): 191-205. [3] Marshall, C. P. and A. O. Marshall (2011). "Hematite and carbonaceous materials in geological samples: A cautionary tale." Spectrochimica Acta Part A: Molecular and Biomolecular Spectroscopy 80(1): 133-137. [4] Bailey, J. V., T. D. Raub, A. N. Meckler, B. K. Harrison, T. M. D. Raub, A. M. Green and V. J. Orphan (2010). "Pseudofossils in relict methane seep carbonates resemble endemic microbial consortia." Palaeogeography, Palaeoclimatology, Palaeoecology 285(1–2): 131-142. [5] Brasier, M. D. and D. Wacey (2012). "Fossils and astrobiology: new protocols for cell evolution in deep time." International Journal of Astrobiology 11(4): 217-228. [6] Wacey, D. (2009). Early Life on Earth: A Practical Guide, Springer. [7] Marshall, C. P., H. G. M. Edwards and J. Jehlicka (2010). "Understanding the Application of Raman Spectroscopy to the Detection of Traces of Life." Astrobiology 10(2): 229-243. [8]ESA (2015). http://exploration.esa.int/mars/45103-rover-instruments/?fbodylongid=2130. [9]NASA (2014). http://mars.nasa.gov/mars2020/mission/instruments/. [10] Marshall, C. P. and A. Olcott Marshall (2013). "Raman hyperspectral imaging of microfossils: potential pitfalls." Astrobiology 13(10): 920-931. [11] Bower, D. M., A. Steele, M. D. Fries and L. Kater (2013). "Micro Raman Spectroscopy of Carbonaceous Material in Microfossils and Meteorites: Improving a Method for Life Detection." Astrobiology 13(1): 103-113. [12] Schopf, J. W. and A. B. Kudryavtsev (2009). "Confocal laser scanning microscopy and Raman imagery of ancient microscopic fossils." Precambrian Research 173(1-4): 39-49. [13] Schopf, J. W. and A. B. Kudryavtsev (2014). Biogenecity of Earth's Earliest Fossils. New York, Springer. [14] Schopf, J. W., A. B. Kudryavtsev, D. G. Agresti, T. J. Wdowiak and A. D. Czaja (2002). "Laser-Raman imagery of Earth's earliest fossils." Nature 416: 73-76. [15] Crosby, C. H., J. V. Bailey and M. Sharma (2014). "Fossil evidence of iron-oxidizing chemolithotrophy linked to phosphogenesis in the wake of the Great Oxidation Event." Geology 42(11): 1015-1018. [16] Fries, M. and A. Steele (2011). Raman Spectroscopy and Confocal Raman Imaging in Mineralogy and Petrography. Confocal Raman Microscopy. T. Dieing, O. Hollricher and J. Toporski, Springer Berlin Heidelberg. 158: 111-135. [17] Foucher, F. and F. Westall (2012). "Raman Imaging of Metastable Opal in Carbonaceous Microfossils of the 700–800 Ma Old Draken Formation." Astrobiology 13(1): 57-67. [18] Emry, J. R., A. O. Marshall and C. P. Marshall (2015). "Evaluating the Effects of Autofluorescence during Raman Hyperspectral Imaging." Geostandards and Geoanalytical Research DOI: 10.1111/j.1751-908X.2015.00354.x. [19] Sasic, S. and Y. Ozaki (2010). Raman, Infrared, and Near-Infrared Chemical Imaging. New Jersey, Wiley.

Misidentification due to Flourescence

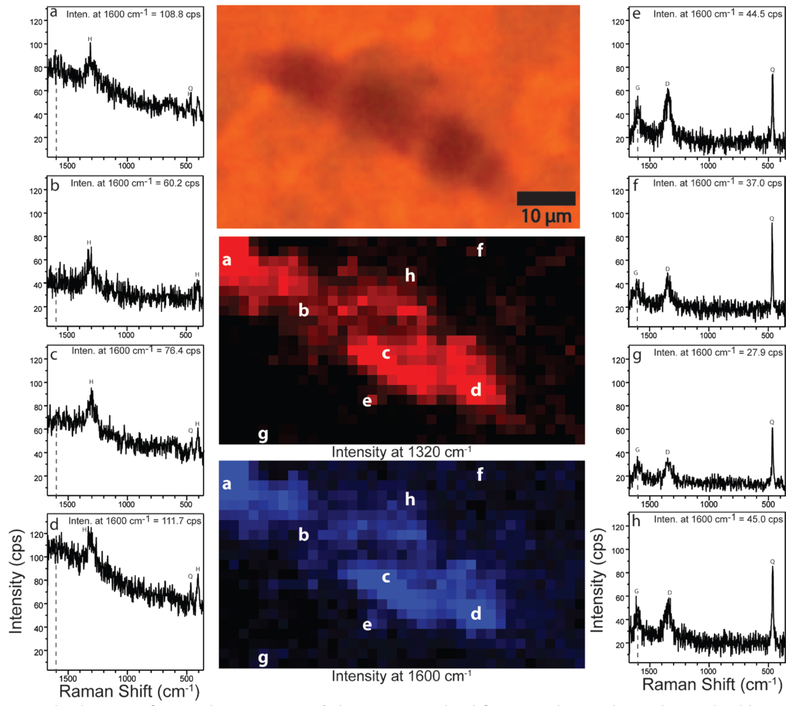

Raman intensity at a point images from a hyperspectral dataset acquired from an Apex chet microvein. Note the high baselines due to autoflourescence in the hematite spectra (a-d) and the relatively low/flat baselines in the mixed quartz-carbon spectra from the matrix. Adapted from [18]

- **Hematite and carbon images appear strikingly similar increasing the potential of misidentifying materials**
- **Ambiguity arises from high sloping baselines generated by autoflourescence in the hematite spectra**
- **Autoflourescence yields false-positive identification of carbon in the "G" band image (1600 cm^{-1})**

Direct Classical Least Squares Analysis

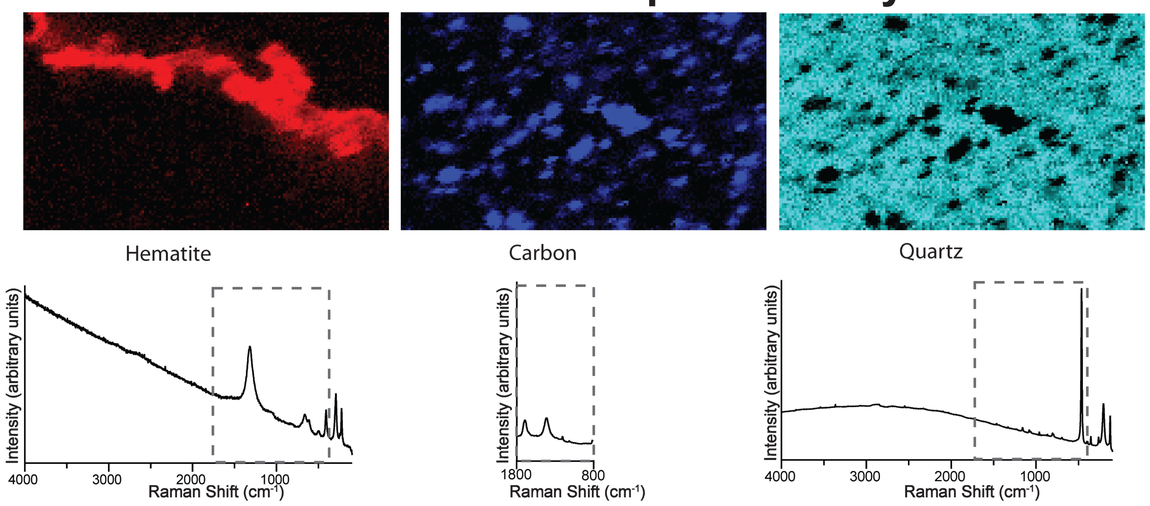

Direct Classical Least squares (DCLS) images for hematite, carbon and quartz for an Apex chert microvein. The images were generated from the analysis based on the reference spectra above. The dashed boxes indiate the portion of the reference spectra utilized in the calculation.

- **Multivariate statistical calculation of the relative contribution of reference spectra to the dataset spectra**
- **Less affected by autoflourescence issues compared to univariate techniques [19]**
- **Provides a complmentary techique with univariate analyses to verify the spatial distribution of materials**

Multiple Analytical Techniques

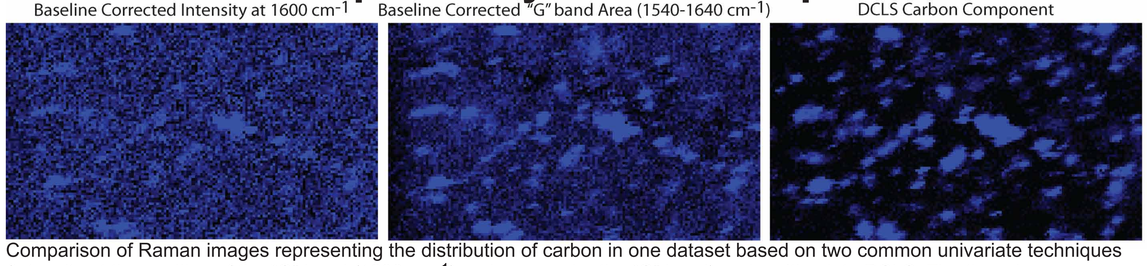

Comparison of Raman images representing the distribution of carbon in one dataset based on two common univariate techniques (intensity at the position of the "G" band (1600 cm^{-1}) and area under the "G" band) and multivariate DCLS. The three images support the interpretation of the presence of carbon in the sample matrix.

- **Issues arising from data quality and analytical techniques require significant consideration**
- **Implementing multiple analytical techniques on a single dataset can provide more robust interpretation**